Applied Energy 228 (2018) 289–300

Contents lists available at ScienceDirect

Applied Energy

journal homepage: www.elsevier.com/locate/apenergy

On the accuracy of CORDEX RCMs to project future winds over the Iberian Peninsula and surrounding ocean

F. Santos[a,b,*], M. Gómez-Gesteira[a], M. deCastro[a], J.A. Añel[a], D. Carvalho[c,d], Xurxo Costoya[b], J.M. Dias[b]

[a] Environmental PHYsics LABoratory (EPHYSLAB), Facultade de Ciencias, Universidade de Vigo, 32004 Ourense, Spain
[b] CESAM – Department of Physics, University of Aveiro, Campus Universitário de Santiago, Aveiro, Portugal
[c] Global Modeling and Assimilation Office (GMAO), NASA Goddard Space Flight Center, Greenbelt, MD 20771, USA
[d] Goddard Earth Sciences Technology and Research (GESTAR), Universities Space Research Association (USRA), Columbia, MD 20771, USA

HIGHLIGHTS

- The skill of CORDEX models to reproduce wind over the Iberian Peninsula.
- CORDEX RCMs showed a higher skill than CMIP5 GCMs to reproduce *in-situ* data.
- CORDEX wind speed was projected for the 21st century showing an overall decrease.
- Wind increase is only projected at some isolated locations.

ARTICLE INFO

Keywords:
Wind offshore and inland
Wind farm
Climate change
CORDEX
CMIP5
Iberian Peninsula

ABSTRACT

The accuracy of CORDEX regional models to reproduce wind speed was assessed at 15 wind farms (216 wind turbines) and 13 oceanic buoys covering the Iberian Peninsula and surrounding ocean during 2012. Models were able to reproduce with relative accuracy both the mean wind speed, with a mean error of 19% inland and 10% offshore, and the wind distribution, with an overlap percentage between distributions of 82 ± 5% inland and 83 ± 3% offshore. In addition, CORDEX regional models showed a skill higher than CMIP5 general models.

Wind speed and wind power were projected over the Iberian Peninsula (Spain and Portugal) and the surrounding ocean for three future periods: near future (2019–2045), midterm (2046–2072) and far future (2073–2099) both at annual and seasonal scales. Both wind speed and wind power will decrease over most of the area with the exception of some regions as: Galicia; the Atlantic coast of Galicia and north of Portugal; the Ebro Valley; the upper Douro Valley; the Guadalquivir Valley; the Strait of Gibraltar and Cape Gata where both will tend to increase. This increase is projected to occur mostly during summer except at the Strait of Gibraltar where it will occur all year long. The change in wind speed and power is higher as farthest the future period is.

1. Introduction

The use of renewable energies has proven to be one decisive solution to counteract human- induced climate change produced by the continuously increase of greenhouse gas emissions, mainly originating from electricity generation from fossil fuels [1]. The presently installed wind power capacity, its fast growth and technological maturity make wind energy the second leading renewable energy source to supply electricity after hydropower. Global wind energy installed capacity was around 539 GW at the end of 2017, from which 177.5 GW are located in Europe [2]. The installed wind power capacity meets 11.6% of the EU's power demand and more than 20% in many countries [3]. WindEurope's *Central Scenario* projects a production of 888TWh of electricity, which is equivalent to 30% of the EU's power demand, by 2030 [4]. Kinetic energy from wind is converted into electricity by wind turbines, most of them grouped in farms, both inland and offshore. Although currently offshore wind energy represents only a small percentage (3.5% in 2017) of the total installed wind energy productive capacity [2], offshore sites have considerable advantages such as higher wind speed with lower turbulence and variability, availability of larger areas for wind farms, lower visual impact from the coast, … Europe has 92% of the global offshore wind installations, resulting in a total cumulative wind power that reached 15.8 GW in 2017 [2,3]. WindEurope's

* Corresponding author at: Environmental PHYsics LABoratory (EPHYSLAB), Facultade de Ciencias, Universidade de Vigo, 32004 Ourense, Spain.
E-mail address: fsantos@uvigo.es (F. Santos).

https://doi.org/10.1016/j.apenergy.2018.06.086
Received 15 February 2018; Received in revised form 24 May 2018; Accepted 17 June 2018
Available online 26 June 2018

Central Scenario projects an installed offshore wind energy capacity of 150 GW by 2030, about 30% of the total European electricity demand [4]. However, there are still many technological challenges in the installation of offshore wind farms. The exploitation of offshore wind is restricted to shallow waters (40–50 m depth), as in the North Sea (67% of the total offshore wind energy production), making that only 19% of the total offshore wind energy production is located in the Atlantic, while the Baltic Sea accounts for 13%. Nevertheless, current research is focused on the development of wind turbines on floating platforms that allows their installation on waters deeper than 60 m [5].

Spain is the fifth country in wind power production worldwide after China, United States, Germany and India, with an installed power close to 23.2 GW at the end of 2017. Wind turbines are grouped in 985 wind farms on land (http://www.thewindpower.net/). In addition, wind was the first renewable energy in electricity supply in 2015 with a share of 19% of the electricity demand, covering the demand of 10 million households and avoiding the emission of 25 million tons of $C0_2$ per year (http://www.aeeolica.org/). In this sense, wind energy represents for Spain the security of energy supply, autonomy, industrial development and environmental sustainability, among others. Portugal is also one of the world leading countries in installed wind generating power. About 24% of its total energy consumption came from wind power alone in 2014, making Portugal the second country in the world in terms of wind power contribution to the total energy consumption. The Iberian Peninsula, as a whole, is one of the regions of the world with more installed wind power per capita and where the wind energy plays a key role in the renewable energy mix.

Synoptic wind patterns are highly dependent on future climate changes, which ultimately will affect wind energy production. It is also well known that a good planning of the future energy mix depends on the impacts of climate change on future power production and demand [6]. Such planning must be based on reliable climate projections, with models that have previously contrasted their accuracy against real data. Future mean wind speed variations and their geographical distribution have a direct impact on wind energy production at regional scale, making some regions more attractive to install wind farms than others. Global Climate Models (GCMs) have shown to be a vital tool to simulate and project the impact of future climate change on wind circulation patterns (IPCC reports). In particular, GCMs from the Coupled Model Intercomparison Project Phase 5 (CMIP5) incorporate additional components that describe the interaction between the atmosphere, land- use and vegetation, taking also into account atmospheric chemistry, aerosols and carbon cycle [7]. GCMs reproduce the main characteristics of general wind patterns, but given their coarse resolution (1.25–2.8°) they are unable to provide accurate wind information at regional scales where the topography, mesoscale meteorological processes and atmosphere-land/ocean surface interface mechanisms must be better resolved, among others. In particular, the potential impacts of climate change on European wind energy resource was analyzed under CMIP5 future climate projections [8]. This study highlights that due to the uncertainty associated to global models projections, further research focused on future trends of wind energy must be carried out by downscaling CMIP5 GCMs output to regional-local scales with regional circulation models (RCMs), to better reproduce the topography, land use and other smaller scale meteorology processes, thus improving wind modeling results. This limitation was overcome by means of different regional downscaling initiatives using both dynamical and statistical downscaling procedures [9–15]. The Coordinated Regional Climate Downscaling Experiment (CORDEX) is the newest and largest ensemble of RCMs, using as forcing the state-of-the-art GCMs from the CMIP5 project under different regional climate change scenarios (regional RCPs) [16]. The CORDEX project has more ensemble members, emission scenarios and higher spatial resolution than its predecessors (PRUDENCE and ENSEMBLES projects).

During the last decade, climate impact on wind and wind power generation in Europe has been analyzed both at global and at regional scales by means of ensembles of GCMs or RCMs under different greenhouse emission scenarios, within the framework of PRUDENCE, ENSEMBLES, CORDEX and CMIP5 projects. An increase in wind speed, extreme wind speed, wind energy and wind potential over northern and central Europe over the 21st century was found in several studies [8,17–26]. Some of these authors found that this increase will be more pronounced during winter [11,13,17,18]. Additionally, [8,19–23] also showed a decrease over Southern Europe or Mediterranean areas. For the Mediterranean region, some authors [10,24] have detected an increase in wind speed or wind potential over land and a decrease over the sea for 2071–2100 and 2061–2090 periods, with the exception of a noticeable increase over the Aegean, Alboran Seas and the Gulf of Lion, together with a greater seasonality.

At a regional scale a remarkable increase in wind energy has been projected over Ireland during winter, although with a decrease during summer over the period 2030–2060 [25]. In the United Kingdom, a decrease in geostrophic wind trend from May to August and an increase in January and from September to November was found from 2081 to 2100 [26]. These authors also concluded that ensemble runs of multiple GCMs could be appropriate since the climate change impact on wind production is highly dependent on the scenario, the modeling process and on the empirical relationship between geostrophic wind and wind potential. Finally, [27] concluded that global warming will not change large- scale winds in the Netherlands and the North Sea along the 21st century beyond the natural climate variability experienced in the past.

Previous studies dealing with future wind speed variability in Spain show a significant decrease over most of the country for the periods 2005–2050 and 2030–2050 [14]. In addition, a significant decrease in future wind energy potential has been also obtained over most of Iberia from 2041 to 2070 [28]. Both studies consider only wind variability over land by means of one RCM with a spatial resolution of 20 km (COSMO in [28]) or by means of an ensemble of RCMs in the A1B scenario with a spatial resolution of 25 km [14]. However, it is necessary to take into account that future wind speed variability at regional scale can be highly dependent on the horizontal resolution, the scenarios, the quality of wind measurements and the RCMs used, as [14] stated in their discussion section. Future offshore wind resources were also analyzed in Western Iberian [29] from 2071 to 2100 by means of an ensemble composed by six RCMs driven by fourteen GCMs under the RCP4.5 and RCP8.5 scenarios, within the framework of CORDEX. The authors found a reduction in wind speed and wind power for all seasons except summer. For the particular case of the Canary Islands, a significant decrease in mean wind speed and wind power was found during summer except in some regions affected by abrupt topographic changes, where a significant increase was detected [15]. This study was carried out by means of an ensemble of fourteen GCMs from the CMIP5 project under the RCP4.5 and RCP8.5 scenarios for 2045–2054 and 2090–2099 future periods.

To validate wind energy simulations at regional scale is a difficult task because wind is highly variable both in time and space and there is a lack of observational wind data collected in wind farms due to commercial confidentiality. In this sense, free reanalysis data [30,31] and meteorological stations [14,15] have been often used instead of wind farms *in situ* observational data to evaluate RCMs ensembles. However, it is known that reanalyses have biases and can differ significantly from observational data in certain regions [30]. This fact was overcome in previous studies by using simple statistical calibrations to correct these biases, both for small geographical regions [32–34] and for Europe as a whole [31]. Meteorological stations provide a valuable information although they have also their own limitations since the measurement height is usually 10 m and not the typical hub height. Additionally, meteorological stations are scattered and most of them located in airports, where wind conditions are very different from those in the areas selected to build up wind farms. In the particular case of the Iberian Peninsula, the Weather and Research Forecasting (WRF) model skill to reproduce wind speed and wind energy production was analyzed comparing with measuring stations inland [35,36,38] and buoys offshore [37,38]. In addition, more recently, offshore wind speed and wind power from an ensemble of CORDEX RCMs

and WRF simulations was evaluated against wind buoys measurements and wind observations from CCMP data [29].

The aim of the present study is to analyze the skill of an ensemble of regional climate models provided by CORDEX to reproduce wind speeds at some specific locations where wind farms and ocean buoys are presently placed in the Iberian Peninsula. The validation of the projection for the immediate future will be carried out by means of experimental wind data measured at thirteen buoys located along the Iberian coast from 2006 to 2016 and at fifteen wind farms scattered throughout the Spanish territory during 2012. As far as we know, this kind of validation of RCMs projections with experimental wind data both inland and offshore is unprecedent.

The skill of CORDEX models will also be compared with the skill of global CMIP5 models (with a much coarser resolution). Finally, near (2019–2045), midterm (2046–2072) and far (2073–2099) future projections of wind speed and wind power will be analyzed both at annual and seasonal scale to determine the impact of climate change on regional winds, both inland and offshore. Results from validations allow inferring the reliability of simulations and models for future scenarios and the suitability of future projections to estimate wind resources along the 21st century.

2. Data and methods

2.1. CORDEX and CMIP5 data

Daily 10 m wind speed were obtained from nine RCMs simulations carried out within the framework of CORDEX project (http://www.euro-cordex.net/) for the Iberian Peninsula region (Fig. 1), at a spatial resolution of 0.11° × 0.11°. The regional simulations were produced by means of four RCMs forced by five different GCMs under the RCP8.5 future emission scenario (Table 1). Historical RCMs simulations (1976–2005) were also considered for comparisons purposes.

In addition, daily 10 m wind speed were also obtained from twenty GCMs simulations carried out within the framework of CMIP5 project (http://cmip-pcmdi.llnl.gov/cmip5/) under the RCP8.5 scenario for the same region, with a spatial resolution that depends on the model but that it is never finer than 1° × 1° (Table 2).

Three different periods of time were considered for future wind speed and power projections: near future (2019–2045), midterm (2046–2072) and far future (2073–2099). Although the far future can be considered as a theoretical wind or power projection because of the typical lifetime of wind turbines, it is necessary to take into account that the lifetime of wind farms is much higher, since existing wind farms are usually subjected to frequent replacement and updates of wind turbines.

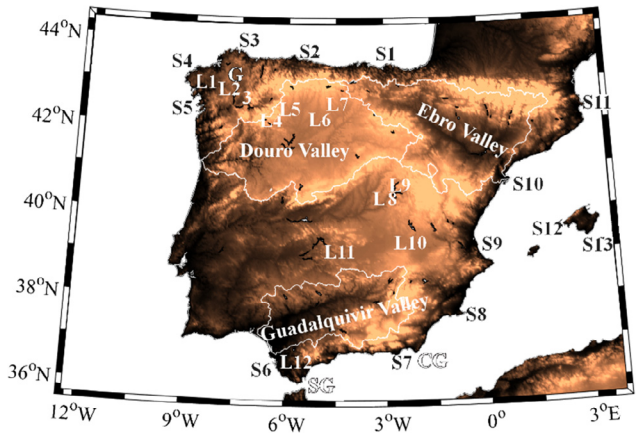

Fig. 1. Area under study including the main toponyms: Galicia (G), Strait of Gibraltar (SG), Cape Gata (CG). Positions labeled with L correspond to wind farms locations and with S to buoys locations.

Table 1
Regional climate simulations from CORDEX (http://www.cordex.org/) project used in this study.

GCMs	RCMs			
	RCA4	RACMO22E	HIRHAM5	CCLM4-8–17
MPI-ESM-LR	M1			
HadGEM2	M2			
IPSL_CM5A	M3			
EC-EARTH	M4	M5	M6	M7
CNRM-CM5	M8			M9

Table 2
Spatial resolution of the global climate models (GCMs) from the CMIP5 project (http://cmip-pcmdi.llnl.gov/cmip5/) used in this study.

GCMs	Resolution (lat × lon)	GCMs	Resolution (lat × lon)
ACCESS1-0	1.25 × 1.87	IPSL-CM5A-LR	1.89 × 3.75
ACCESS1-3	1.25 × 1.87	IPSL-CM5A-MR	1.27 × 2.5
CMCC-CESM	3.44 × 3.75	IPSL-CM5B-LR	1.89 × 3.75
CMCC-CMS	3.71 × 3.75	MIROC-ESM-CHEM	2.79 × 2.81
CNRM-CM5	1.40 × 1.41	MIROC-ESM	2.79 × 2.81
CanESM2	2.79 × 2.81	MIROC5	1.40 × 1.41
GFDL-CM3	2 × 2.5	MPI-ESM-LR	1.87 × 1.87
HadGEM2-CC	1.25 × 1.87	MPI-ESM-MR	1.87 × 1.87
HadGEM2-ES	1.25 × 1.87	MRI-CGCM3	1.12 × 1.12
INMCM4	1.5 × 2	MRI-ESM1	1.12 × 1.12

2.2. Field data

Field data consists of wind observations collected by thirteen buoys distributed along the Spanish coast (Peninsula and Balearic Islands) and by fifteen wind farms, with a total of 216 wind turbines distributed inland all over Spain (Tables 3 and 4 and Fig. 1, numbers).

Wind data from wind farms were provided by Gas Natural Fenosa Renovables (www.gasnaturalfenosa.com) with a time resolution of 10 min over the year 2012. Wind time series from each turbine is considered only if the number of invalid values (voids and unrealistic data) is less than 10% to assure data quality. Additionally, the mean of all turbines is calculated for each wind farm. Only those turbines with wind values within the interval $\overline{W} \pm 2\sigma$ are considered, being $\overline{W}$ the mean wind time series of all turbines and σ the standard deviation. Only three turbines were discarded from the analysis previously described, which shows the good performance of the wind measuring instruments

Table 3
Location of wind farms provided by Gas Natural Fenosa Renovables (www.gasnaturalfenosa.com) and distributed all over the Iberian Peninsula (left numbers correspond to their position in Fig. 1). The last column represents the number of turbines in each wind farm.

Number	Wind farm	Latitude (°N)	Longitude(°E)	Number of turbines
L1	Silvaredonda	43.15	351.19	7
L2	Codesas I	42.97	352.02	20
L3	Codesas II	43	351.9	25
L4	Val de Lín	42.54	353.69	9
L5	Val de la Casa	42.63	353.91	6
L6	Val de Pero	42.01	355.49	15
L7	Montejo	42.93	356.11	15
L8	Canredondo	40.82	357.48	13
L9	Peña I	40.99	358.09	8
	Loma Gorda			25
	San Gil			18
L10	La Losilla	39.06	358.19	9
L11	Malagón I, II	39.28	356.11	17 + 25
L12	Las Vegas	36.47	353.51	4

Table 4
Location of buoys provided by Puertos del Estado (http://www.puertos.es/) and distributed around the Iberian Peninsula and Baleares Islands. Left numbers correspond to their position in Fig. 1.

Number	Buoy	Latitude (°N)	Longitude (°E)
S1	Bilbao	43.64	356.95
S2	Cape Peñas	43.75	353.84
S3	Estaca de Bares	44.12	352.31
S4	Sisargas	43.50	350.8
S5	Cape Silleiro	42.12	350.57
S6	Gulf of Cádiz	36.48	353.04
S7	Cape Gata	36.57	357.68
S8	Cape Palos	37.65	359.67
S9	Valencia	39.52	0.21
S10	Tarragona	40.68	1.47
S11	Begur	41.92	3.65
S12	Dragoneras	39.46	2.1
S13	Mahón	39.72	4.42

and reliability of its data. The coordinates of the wind farms are described in Table 3 and depicted in Fig. 1 (labelled with L). Table 3 also contains the number of wind turbines available for each wind farm (right column). Hourly wind data covering the period 2006–2016 were obtained from marine buoys deployed by Puertos del Estado (http://www.puertos.es/). These buoys sample at a height of 3 m above sea level and their coordinates are described in Table 4 and depicted in Fig. 1 (labelled with S).

Wind farms very close to each other are numbered with the same number since they are undistinguishable with CORDEX resolution. This is the case of Peña I, Loma Gorda and San Gil wind farms which are numbered with number L9 or Malgón I and II which are numbered with number L11 in tables and Fig. 1.

2.3. Methods

Wind data from buoys are extrapolated to 120 m, the typical hub height of offshore wind turbines. CORDEX and CMIP5 data are extrapolated to 80 m or 120 m, which corresponds to the typical hub height of wind turbines on land and offshore, respectively. The optimal wind extrapolation should be done with methods that account for the atmospheric stability, such as the Monin-Obukhov theory [39] or the Liu and Tang method [40]. However to apply these methods it would be necessary measurements of temperature, heat fluxes and friction velocity that the buoys considered in the study do not collect, as it was explained in detail in [37,38]. In the absence of such data, the wind extrapolation is carried out assuming a logarithmic wind profile that assumes a neutrally stratified atmosphere [41], following the expression previously applied by [10,42]:

$$W_H = W_{ns}\frac{\ln\left(\frac{H}{z_0}\right)}{\ln\left(\frac{H_{ns}}{z_0}\right)} \quad (1)$$

H represents the hub height of the wind turbine on land and offshore; H_{ns} is the height at which near surface winds are measured (10 m for CORDEX and 3 m for buoys); W_H is the wind speed at the hub height; W_{ns} is the near surface wind speed and z_0 the roughness length. z_0 for each wind farm on land is obtained from [41] once the land-use category was retrieved from the Spanish National Geographic Institute (http://www.ign.es). At ocean locations a value of $z_0 = 0.001$ m is considered for open calm sea [43,44].

The wind power (WP) of a turbine depends on the air density, wind velocity and on the characteristics of each wind turbine model (as the turbine radius and the rotor power coefficient). The specific cut-in velocity is about 3 ms^{-1} and the cut- out velocity is 28 ms^{-1} for most of the wind turbine models installed throughout the Iberian Peninsula [28]. The WP per unit area perpendicular to the wind flow (the wind energy flux) between the turbine specific cut-in and the rated wind velocity is expressed following [10,12] by the equation:

$$WP = \frac{1}{2}\rho W_H^3 \quad (2)$$

where ρ is the air density (1.225 kg m^{-3} at 15 °C and 100 kPa).

The skill of the RCM ensemble to predict future wind is statistically analyzed in terms of the mean wind ($\langle W\rangle$) and the percentage of overlap between measured and modelled probability distribution functions (OP). Only a statistical study can be carried out because historical RCMs models run using GCMs as boundary conditions and, therefore, their climate is not synchronized with the measured climate, especially at daily scales.

$\langle W\rangle_M$ is the mean wind speed of all models, which is calculated by computing the mean wind projected by each model at any location and then averaging over the models. The standard deviation of the models (σ_M) is calculated in the same way. $\langle W\rangle_F$ is the mean wind speed at each farm, which is calculated as $\langle W\rangle_M$ but averaging over the turbines instead of over the models. The same protocol is followed to calculate the standard deviation of the wind speed for each farm (σ_F). $\langle W\rangle_B$ is the mean wind speed at any single buoy.

The percentage of error (EP) between projected and field data is calculated for any model M_i at any location j as

$$EP_{M_i}^j = 100 \times \frac{\langle W\rangle_{M_i} - \langle W\rangle_{in\ situ}}{\langle W\rangle_{ref}} \quad (3)$$

where the subscript *in situ* refers to farms or buoys and ref to a reference value that is calculated as the average between measured and projected means

$$\langle W\rangle_{ref} = \frac{\langle W\rangle_{M_i} + \langle W\rangle_{in\ situ}}{2} \quad (4)$$

The root mean square error and the bias of the error percentage are calculated over models or stations following

$$EP_{RMSE} = \left[\frac{1}{N}\sum_{k=1}^{N}\left(EP_{M_i}^j\right)^2\right]^{1/2} \quad (5)$$

$$EP_{Bias} = \frac{1}{N}\sum_{k=1}^{N} EP_{M_i}^j \quad (6)$$

where k and N can refer to the stations or to the models.

Although traditionally most of the analyses evaluate the skill of climate models in terms of means and standard deviations, this approach does not allow the comparison of the whole data distribution. In fact, a good simulation of the mean does not ensure that the main features of the data set are satisfactorily captured by the models [45]. In addition, metrics based on mean values can mask biases or systematic errors that would be observable at daily scale. Thus, a procedure similar to the one described in [45] is followed to analyze the OP between the probability distribution function (PDF) projected by models and measured *in situ*. Models reproducing perfectly *in situ* data will make both PDFs coincident with an OP equal to 100%.

Wind changes projected by CORDEX under the RCP8.5 scenario along the 21st century (2006–2099) are calculated from wind trends. Trends are computed by linear fitting of wind versus time at the location of each buoy and wind farm. Then, trends are multiplied by the number of years to obtain the changes. The significance of each model is evaluated by applying the Spearman's correlation due to its robustness to outliers. Daily wind values can be affected by temporal autocorrelation, in such a way that the real number of degrees of freedom (N_{eff}) is much smaller than the sample size (N). The degrees of freedom are calculated using the Quenouille procedure [46], following [47]. In this way, N_{eff} is calculated following $N_{eff} = N(1-r_1)/(1+r_1)$, where r_1 is the lag-1 autocorrelation coefficient of the series. In addition, a consensus among RCMs is considered when at least two thirds of the

Table 5
Mean wind averaged for all models ($\langle W\rangle_M$), mean wind averaged over the turbines of each farm ($\langle W\rangle_F$) and mean wind at each buoy location ($\langle W\rangle_B$). All data was calculated on 2012 and they are in ms^{-1}. σ represents the standard deviation of models (σ_M) and wind farms (σ_F).

# Farm	$\langle W\rangle_M \pm \sigma_M$	$\langle W\rangle_F \pm \sigma_F$	# Buoy	$\langle W\rangle_M \pm \sigma_M$	$\langle W\rangle_B$
L1	8.0 ± 1.2	6.7 ± 0.8	S1	6.4 ± 0.4	6.5
L2	8.2 ± 1.7	6.5 ± 0.9	S2	6.7 ± 0.4	6.8
L3	7.8 ± 1.5	6.3 ± 0.8	S3	9.0 ± 0.4	8.5
L4	6.1 ± 1.5	5.3 ± 0.6	S4	9.5 ± 0.4	8.7
L5	6.2 ± 1.6	6.2 ± 0.6	S5	8.5 ± 0.6	7.7
L6	5.8 ± 0.4	6.1 ± 0.7	S6	7.6 ± 0.3	7.3
L7	7.1 ± 1.4	5.5 ± 0.9	S7	8.2 ± 0.6	6.7
L8	5.9 ± 0.7	7.2 ± 0.7	S8	6.5 ± 0.4	5.9
L9	6.9 ± 0.9	7.1 ± 1.1	S9	5.2 ± 0.3	6.3
	6.9 ± 0.9	7.1 ± 0.8	S10	5.9 ± 0.4	5.7
	6.9 ± 0.9	6.5 ± 0.7	S11	8.2 ± 0.7	8.9
L10	5.4 ± 0.6	5.6 ± 0.7	S12	5.9 ± 0.2	6.2
L11	6.0 ± 0.5	5.5 ± 0.8	S13	7.0 ± 0.3	6.8
	6.0 ± 0.5	5.3 ± 0.7			
L12	6.6 ± 0.6	6.0 ± 0.5			

models present the same sign of change and at least half of those models have a significance higher than 90%.

3. Results and discussion

3.1. Skill of CORDEX RCMs to reproduce winds

First of all, the skill of the RCMs to predict wind speed were analyzed in terms of the mean wind values. Table 5 shows the mean and the standard deviation of wind speed calculated both *in situ* (farms and buoys) and with CORDEX RCMs at the same locations. In general, the standard deviations are lower at water locations, where topography (which can be different for each model) is obviously less important. In addition, all *in situ* values (except S7 and S9) are in the interval $\langle W\rangle_M \pm 2\sigma$. The percentage of error of each model in reproducing mean winds over land is depicted in Table 6. Note that the difference was always calculated as modelled wind minus measured wind, as mentioned above. When looking at the error of the speed (in absolute value), from the available 135 cases (9 models × 15 farms), errors higher than 50% were observed in just 1 case, higher than 40% in just 6 cases and higher than 30% in 23 cases. RMSE and bias percentages were calculated both for models and for stations. There is a non-negligible difference between the performance of the different models (last two rows) with RMSEs ranging from 10% (EC-EARTH-RCA4) to 29% (EC-EARTH-RACMO22E) and biases ranging from −11% (IPSL-CM5A-RCA4) to 19% (HadGEM2-RCA4). EP is also dependent on the location (last two columns) with RMSEs ranging from 9% (location L6) to 30% (location L7) and a biases ranging from −20% (location L8) to 23% (location L7). Overall, both the biases (5%) and the RMSEs (19%) are moderate when considering all wind farms and models.

Table 7 is similar to Table 6 but for offshore locations. Here, the percentage of error (in absolute value) never surpasses 30%. All models show a similar performance (last two rows) with RMSEs ranging from 9% (MPI-ESM-LR-RCA4, IPSL-CM5A-RCA4 and CNRM-CM5-RCA4) to 14% (CNRM-CM5-CCLM4-8-17) and biases ranging from −2% (MPI-ESM-LR-RCA4) to 6% (HadGEM2-RCA4 and EC-EARTH-RCA4). Results are also dependent on the location (last two columns) as previously observed for farms, with RMSEs ranging from 4% (location S13) to 21% (location S7) and biases ranging from −18% (location S9) to 20% (location S7). Overall, both the bias (2%) and the RMSE (10%) are small when considering all buoys and models. In addition, these values are considerably lower than previously described for inland farms, showing that the performance of CORDEX RCMs is higher at ocean locations, as it would be expected. Both tables are summarized in Fig. 2.

As we mentioned above, the use of metrics such as means and standard deviations does not allow comparing the full data distribution. Thus, a procedure based on probability density functions was considered [45] and the skill of RCMS to predict wind speed was assessed by means of the overlap percentage between measured and modeled data (Table 8). Overall, the mean overlap percentage (last row) is similar for all models, ranging from 77 ± 10% (EC-EARTH-RACMO22E) to 85 ± 4% (MPI-ESM-LR-RCA4). The multi-model mean of the overlap percentage ($\langle OP\rangle_M$, penultimate column) is dependent on the location of the farm, ranging from 76 ± 6% (farm L4) to 88 ± 3% (farm L11). Overall, the mean skill averaged over all models and stations is 82 ± 5%. It should be noted that inland field data are themselves affected by uncertainties, as shown by the mean *intra-farm* overlap percentage ($\langle OP\rangle_F$, last column). This value was calculated as the mean of the overlap percentage among the turbines from the same farm. $\langle OP\rangle_F$ values range from 91 ± 5% to 95 ± 2%, depending on the location, with a mean value close to 94 ± 3%. Thus, comparing the mean overlap of models against wind farms (82 ± 5%) with the mean intra-farm overlap (94 ± 3%), the accuracy of models to reproduce *in situ* data is high.

A similar analysis was carried out to compare CORDEX projections with data from buoys (Table 9). All models (last row) showed a very

Table 6
Percentage of error between mean wind projected for each RCM and mean wind averaged at each wind farm on 2012 ($EP_{M\#}$). EP was calculated as $[(W_p - W_f)/\overline{D}] * 100$ where the subscript f (p) represents farm (projected) data, $\overline{W}$ is the mean value calculated as $(W_p + W_f)/2$. The penultimate (last) column represents the root mean square error (bias) of the EP for the nine RCMs ($\overline{EP}$). The RMSE and bias were also calculated for each model.

Farm	EP_{M1}	EP_{M2}	EP_{M3}	EP_{M4}	EP_{M5}	EP_{M6}	EP_{M7}	EP_{M8}	EP_{M9}	$\overline{EP}_{RMSE}$	$\overline{EP}_{Bias}$
L1	−3	33	−7	6	15	23	30	22	34	22	17
L2	−9	38	−12	−2	36	30	35	28	41	29	21
L3	−7	36	−11	−3	36	29	33	28	39	28	20
L4	−17	35	−23	19	−31	26	31	15	38	27	10
L5	−36	22	−43	4	−43	15	17	2	24	27	−4
L6	−12	0	−13	−8	−10	−5	0	−13	4	9	−6
L7	0	46	−9	29	−1	29	37	30	42	30	23
L8	−16	−9	−22	−11	−51	−17	−16	−24	−11	23	−20
L9	6	9	−9	1	−36	−7	0	−11	9	14	−4
	7	10	−8	2	−35	−6	1	−10	10	14	−3
	16	19	1	11	−26	3	10	−1	19	14	6
L10	−8	3	−7	−6	−21	−2	4	−13	6	10	−5
L11	1	16	1	0	−5	17	15	8	19	12	8
	4	19	4	3	−2	20	18	11	21	14	11
L12	−3	13	−4	−1	22	13	19	12	13	13	9
RMSE	13	25	16	10	29	19	22	18	26	**19**	
Bias	−5	19	−11	3	−10	11	16	6	21		**5**

Table 7
Percentage of error between mean wind projected for each RCM and mean wind at each buoy on 2012 ($EP_{M\#}$). EP was calculated as $[(W_p - W_b)/\overline{D}] * 100$ where the subscript b (p) represents buoy (projected) data, $\overline{W}$ is the mean value calculated as $(W_p + W_b)/2$. The penultimate (last) column represents the root mean square error (bias) of the EP for the nine RCMs ($\overline{EP}$). The RMSE and bias were also calculated for each model.

Buoy	EP_{M1}	EP_{M2}	EP_{M3}	EP_{M4}	EP_{M5}	EP_{M6}	EP_{M7}	EP_{M8}	EP_{M9}	$\overline{EP}_{RMSE}$	$\overline{EP}_{Bias}$
S1	−5	5	−5	9	−12	−3	−2	−4	−3	6	−2
S2	−7	7	−10	0	−12	−3	2	−4	5	7	−2
S3	2	12	3	1	1	6	9	5	12	7	6
S4	5	15	5	5	10	8	11	8	14	10	9
S5	8	18	−2	16	12	6	11	0	13	11	9
S6	9	7	4	2	4	2	1	−3	5	5	3
S7	5	22	16	16	20	24	29	22	27	21	20
S8	−5	8	6	9	18	11	12	10	17	12	10
S9	−27	−17	−23	−14	−24	−15	−16	−16	−12	19	−18
S10	1	8	5	16	−3	−6	−5	0	3	7	2
S11	−9	−6	−8	6	−3	−6	−16	−10	−26	12	−9
S12	−9	−4	−4	2	−6	−2	−9	−6	0	5	−4
S13	−2	5	−1	11	2	5	0	1	3	4	3
RMSE	9	12	9	10	12	10	12	9	14	**10**	
Bias	−2	6	−1	6	1	2	2	0	4		**2**

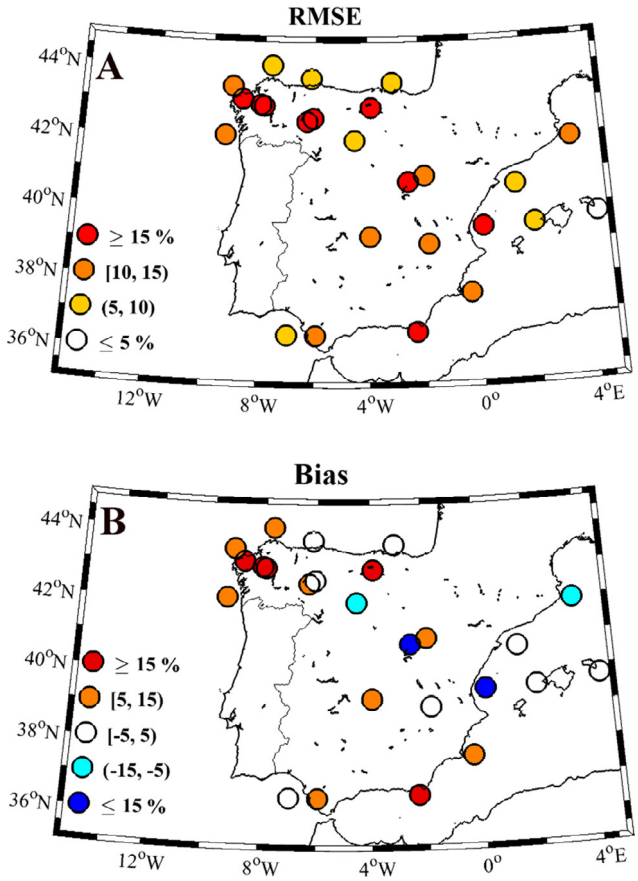

Fig. 2. (A) Root mean square error (RMSE) and (B) bias of the mean percentage of error between mean wind projected by RCMs and mean wind measured *in situ* (farm and buoy) on 2012. The percentage of error was calculated as $[(W_p - W_f)/\overline{D}] * 100$ where the subscript f (p) represents farm (projected) data, $\overline{W}$ is the mean value calculated as $(W_p + W_f)/2$. Circles mark the location of wind farms and buoys. Values are in percentages.

similar skill ranging from 82 ± 3% (HadGEM2-RCA4) to 84 ± 5% (EC-EARTH-CCLM4-8-17). Multimodel values (last column) ranged from 77 ± 2% (location S9) to 87 ± 3% (location S6). The mean skill averaged over all models and buoys was 83 ± 3%, which is slightly higher than observed for inland locations, showing the better performance of RCMs to reproduce offshore winds, where topography an land- use limitations of the models are obviously not an issue. The overlap percentages described for Tables 8 and 9 are summarized in Fig. 3.

A similar analysis was carried over the period 2006–2016 when *in situ* measurements are available at the buoys. Fig. 4 shows the mean OP at ocean locations (Fig. 4a) and the RMSE (Fig. 4b) and bias (Fig. 4c) of EP calculated for all models at ocean locations. The skill of the models to reproduce offshore winds is even higher (RMSEs and biases are lower and the overlap percentages higher) when considering this longer period (compare with ocean locations in Figs. 2 and 3).

3.2. Comparison with the skill of CMIP5 GCMs

The skill of CMIP5 was also analyzed by means of 20 GCMs as described above. Table 10 summarizes the different metrics considered for the analysis, RMSE ($\overline{PE}_{RMSE}$) and bias ($\overline{PE}_{Bias}$) of the percentage of error between modelled and measured data and mean overlap percentage ($\langle OP \rangle_M$) for all available locations (farms and buoys).

When focusing on inland farms, $\overline{PE}_{RMSE}$ ranged from 21% (L12) to 49% (L1) and $\overline{PE}_{Bias}$ from −14% (L6) to 40% (L1). $\langle OP \rangle_M$ ranged from 64 ± 18% (L1) to 78 ± 12% (L11). Overall, the RMSE is 33%, the bias 9% and $\langle OP \rangle_M$ 73 ± 12%. These three metrics show that the skill of CMIP5 GCMs to reproduce inland winds is considerably lower than previously observed for CORDEX (see Tables 6 and 8), as expected given the latter better ability to deal with meso- to local-scale meteorology. Regarding offshore data at buoys, $\overline{PE}_{RMSE}$ ranged from 10% (S12) to 68% (S11) and $\overline{PE}_{Bias}$ from −56% (S11) to 7% (S13). $\langle OP \rangle_M$ ranged from 57 ± 16% (S11) to 81 ± 4% (S13). Overall, the RMSE is 31%, the bias −14% and $\langle OP \rangle_M$ 69 ± 10%. Once again, the skill of CMIP5 models to reproduce inland winds is considerably lower than previously observed for CORDEX models (see Tables 7 and 9). Surprisingly, in general, the performance of models is worst for offshore locations. This is due to the fact that the offshore buoys are located at less than 1 degree from coast and not at the open sea, in such a way that the model cannot satisfactorily distinguish between land and ocean locations due to the coarseness of the grid. In addition, the coarse resolution of GCMs hampers a realistic simulation of localized meteorology near the coast, where medium to small scale processes are relevant due to abrupt changes in topography, roughness and atmospheric conditions (like thermal gradients).

3.3. Annual and seasonal evolution of wind speed and wind power along the 21st century

Once the skill of CORDEX RCMs to reproduce the wind both inland and offshore has been assessed, the impact of climate change on the

Table 8
Overlap percentage of wind calculated for each wind farm and RCM ($OP_{M\#}$) on 2012. The penultimate column represents the average of the overlap percentages for the nine RCMs ($\langle OP\rangle_M$). The last column is the mean of the overlap percentages for the different turbines of the same wind farm ($\langle OP\rangle_F$). MS is the model skill to reproduce wind on land and it was calculated as the spatial mean of the overlap percentages for each model. σ is the standard deviation.

Farm	OP_{M1}	OP_{M2}	OP_{M3}	OP_{M4}	OP_{M5}	OP_{M6}	OP_{M7}	OP_{M8}	OP_{M9}	$\langle OP\rangle_M \pm \sigma$	$\langle OP\rangle_F \pm \sigma$
L1	89	71	89	89	81	82	76	82	72	**81 ± 7**	**93 ± 4**
L2	88	71	82	89	69	78	76	81	68	**78 ± 8**	**91 ± 5**
L3	88	70	84	89	68	77	77	79	69	**78 ± 8**	**93 ± 4**
L4	86	73	74	79	69	81	69	83	71	**76 ± 6**	**95 ± 3**
L5	75	80	68	89	68	82	80	87	80	**79 ± 7**	**94 ± 3**
L6	88	88	90	91	90	90	89	84	91	**89 ± 2**	**94 ± 2**
L7	89	71	88	75	92	79	76	81	71	**80 ± 8**	**92 ± 3**
L8	82	82	79	85	63	82	79	74	83	**79 ± 7**	**95 ± 2**
L9	83	85	85	84	74	89	82	89	81	**84 ± 5**	**95 ± 2**
	85	85	85	85	71	88	80	86	80	**83 ± 5**	**95 ± 2**
	79	79	81	79	74	86	76	86	74	**79 ± 4**	**94 ± 3**
L10	87	85	84	77	83	87	81	82	81	**83 ± 3**	**93 ± 3**
L11	91	87	90	93	89	83	86	92	84	**88 ± 3**	**92 ± 4**
	89	85	88	91	89	84	84	90	84	**87 ± 3**	**95 ± 3**
L12	83	80	85	81	82	79	80	85	87	**82 ± 3**	**95 ± 2**
MS	**85 ± 4**	**80 ± 7**	**83 ± 6**	**85 ± 6**	**77 ± 10**	**83 ± 4**	**79 ± 5**	**84 ± 5**	**78 ± 7**	**82 ± 5**	**94 ± 3**

wind fields along the 21st century was analyzed in terms of wind increment (ΔW), computed at the position of wind farms and buoys (Table 11 and Fig. 5). Values in Table 11 were observed to range from $-0.49\,ms^{-1}$ at Dragoneras (S12 in Fig. 1) to $0.32\,ms^{-1}$ at Las Vegas (L12 in Fig. 1). These increments are around −8.3% and 4.8% of the wind speed offshore and inland respectively, according to the mean values provided by Table 5. White dots inside the circles (Fig. 5) mark locations with a high consensus among models. This consensus was mostly attained at points with negative increments higher (in absolute value) than $0.30\,ms^{-1}$. In general, there is less consensus on wind changes at wind farms (~42% of the points) than at buoys (~62% of the points), probably because the differences among models are smaller offshore, where model lower boundary effects (topography, land use) are not an issue.

The increment in the number of days with wind speed under the cut-in velocity of $3\,ms^{-1}$ (ΔCalms) was calculated along the 21st century at buoys and wind farms locations to assess the future performance of wind farms installed throughout the Iberian Peninsula and its continental shelf (Table 11 and Fig. 6). ΔCalms in Table 11 range from −5 days at Las Vegas (L12 in Fig. 1), which is the station with the highest ΔW, to 14 days at Tarragona and Dragoneras (S10 and S12 in Fig. 1), the stations with the lowest ΔW. Overall, an increase in the number of days under the cut- in velocity is detected both inland and offshore (Fig. 6). Nevertheless, a consensus among models was only observed at a few stations, with an increment in the number of days higher than 7;

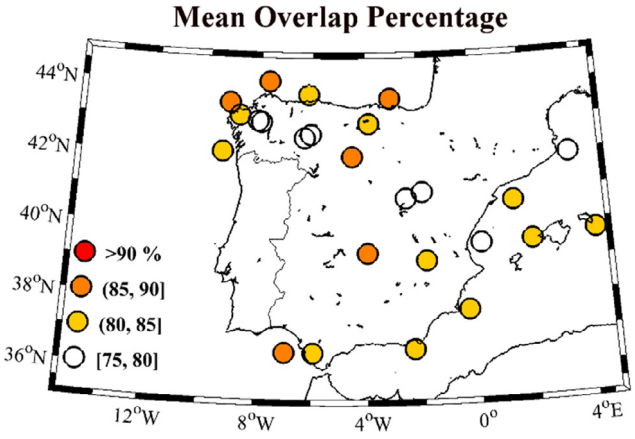

Fig. 3. Mean overlap percentages between projected and *in situ* wind probability density functions both at wind farms and buoys locations on 2012. Circles mark the location of wind farms and buoys.

especially at the eastern part of the Iberian Peninsula and around the Balearic Islands.

The previous analysis is only focused on the locations where wind farms or buoys already exist. Changes in the annual wind speed and wind power were also projected for the whole area. Fig. 7 shows the

Table 9
Overlap percentage of wind calculated for each buoy and RCM ($OP_{M\#}$) on 2012. The last column represents the average of the overlap percentages for the nine RCMs ($\langle OP\rangle_M$). MS is the model skill to reproduce wind offshore and it was calculated as the spatial mean of the overlap percentages for each model. σ is the standard deviation.

Buoy	OP_{M1}	OP_{M2}	OP_{M3}	OP_{M4}	OP_{M5}	OP_{M6}	OP_{M7}	OP_{M8}	OP_{M9}	$\langle OP\rangle_M \pm \sigma$
S1	85	86	84	87	79	86	89	85	85	**85 ± 3**
S2	82	87	83	82	77	82	90	84	87	**84 ± 4**
S3	89	85	88	84	86	86	84	87	82	**86 ± 2**
S4	86	84	85	86	88	87	87	84	83	**85 ± 2**
S5	83	82	82	84	84	83	87	83	83	**83 ± 1**
S6	85	80	85	88	87	87	90	89	87	**87 ± 3**
S7	88	82	87	85	84	83	75	87	79	**83 ± 4**
S8	85	82	86	79	77	81	88	84	83	**83 ± 3**
S9	76	76	75	80	79	76	79	78	78	**77 ± 2**
S10	84	78	84	82	83	82	82	79	78	**82 ± 2**
S11	82	78	79	83	82	75	76	74	74	**78 ± 4**
S12	83	84	84	86	83	83	85	87	85	**84 ± 1**
S13	87	81	84	84	85	78	86	82	81	**83 ± 3**
MS	**84 ± 3**	**82 ± 3**	**84 ± 3**	**84 ± 3**	**83 ± 3**	**82 ± 4**	**84 ± 5**	**83 ± 4**	**82 ± 4**	**83 ± 3**

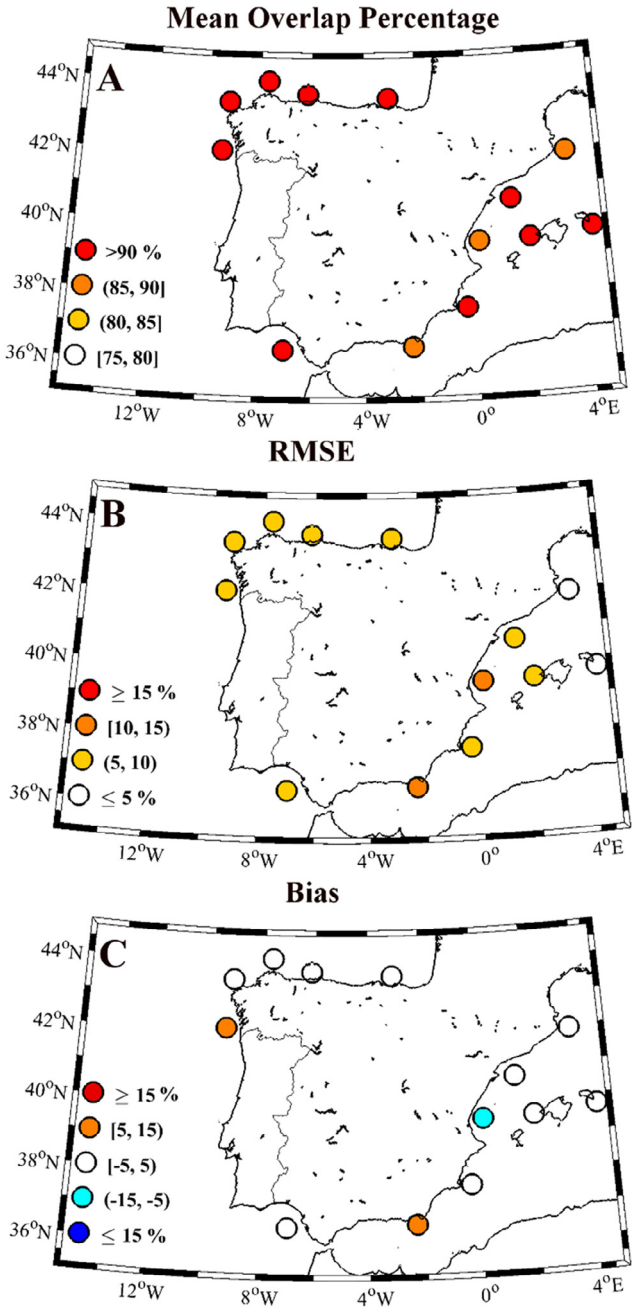

Fig. 4. (A) Mean overlap percentages between projected and *in situ* wind probability density functions at buoys locations from 2006 to 2016. (B) Root mean square error (RMSE) and (C) bias of the mean percentage of error between mean wind projected by RCMs and mean wind at buoys from 2006 to 2016. The percentage of error was calculated as $[(W_p - W_f)/\overline{D}] * 100$ where the subscript f (p) represents farm (projected) data, $\overline{W}$ is the mean value calculated as $(W_p + W_f)/2$. Circles mark the location of wind farms and buoys.

multimodel map of the percentage of change for wind speed (left column) and wind power (right column) between future and historical data. Three future time windows were considered: near future (2019–2045), midterm (2046–2072) and far future (2073–2099). Overall, both wind speed and power is observed to decrease in most of the area, no matter the period under study. The wind speed (power) decrease is lower than 5% (10%) in most of the area under study. Here we will mainly focus on the few areas were wind speed and power will tend to increase. A light increase is observed for the near future (Fig. 7a and b) in the Ebro Valley and at Gibraltar Strait. The percentage of increase is lower than 5% in wind speed and 10% in wind power. No

Table 10
Overlap percentages and error percentages averaged for the twenty GCMs at each wind farm and buoy location on 2012 ($\langle OP \rangle_M$ and $\overline{PE}$, respectively). The RMSE and bias of the PE were calculated for all RCMs ($\overline{PE}_{RMSE}$ and $\overline{PE}_{Bias}$). MS is the skill of the RCM ensemble to reproduce wind on land and offshore calculated as the spatial mean of the $\langle OP \rangle_M$ and $\overline{PE}$. σ is the standard deviation.

# Farm	$\overline{PE}_{RMSE}$	$\overline{PE}_{Bias}$	$\langle OP \rangle_M \pm \sigma$	# Buoy	$\overline{PE}_{RMSE}$	$\overline{PE}_{Bias}$	$\langle OP \rangle_M \pm \sigma$
L1	49	40	64 ± 18	S1	45	−25	65 ± 15
L2	45	32	68 ± 17	S2	36	−6	68 ± 12
L3	47	35	66 ± 18	S3	22	−9	75 ± 10
L4	36	25	73 ± 14	S4	38	−23	66 ± 16
L5	27	11	77 ± 9	S5	15	2	75 ± 7
L6	31	−14	74 ± 9	S6	37	−29	63 ± 13
L7	41	24	69 ± 16	S7	37	−21	69 ± 12
L8	31	−12	70 ± 10	S8	20	1	73 ± 9
L9	32	−12	75 ± 9	S9	32	−21	70 ± 9
	32	−11	73 ± 10	S10	28	−8	66 ± 8
	30	−2	75 ± 11	S11	68	−56	57 ± 16
L10	24	7	73 ± 7	S12	10	6	80 ± 5
L11	25	3	78 ± 11	S13	11	7	81 ± 4
	26	6	78 ± 12				
L12	21	3	76 ± 8				
MS	**33**	**9**	**73 ± 12**		**31**	**−14**	**69 ± 10**

change is observed in wind speed in Galicia and its Atlantic coast, although a small increase in wind power is observed. A similar pattern was observed for the midterm projection (Fig. 7c and d) although at a higher intensity. New increasing spots can be observed in Galicia and its Atlantic coast, in the Guadalquivir Valley and at Cape Gata. This pattern will intensify for the far future (Fig. 7e and f), with some areas showing a percentage of decrease greater than 20% and a percentage of increase higher than 25% at the Strait of Gibraltar. The increasing pattern observed in the Galician area had been previously described for another wind dependent variable like the upwelling index [48]. In this study, wind changes are related to the displacement of the Azores High.

Changes in wind speed and power were also projected along the 21st century at seasonal scales for the far future (2073–2099). Only the far future is considered because, although there are small differences in some regions of the area under study, very similar annual wind speed and power patterns of change are observed for the three future periods. Fig. 8 shows multimodel maps of percentage of change for wind speed (left column) and power (right column) between far future and historical data during winter (DJF, (a–b)), spring (MAM, (c–d)), summer (JJA, (e–f)) and autumn (OND, (g–h)). An overall decrease in wind speed and power is detected in most of the area under study in winter (Fig. 8(a, b)) and autumn (Fig. 8(g, h)). Only a small increase (10%) in wind power is projected offshore, along the Atlantic Iberian coast during autumn. On the contrary, an increase in both variables were projected in several regions of the Iberian Peninsula and the surrounding oceanic areas in spring (Fig. 8(c, d)) and summer (Fig. 8(e, f)). Increments between 5% and 10% in wind speed and between 25% and 30% in wind power were projected in: Galicia; offshore, along the Atlantic Iberian coast; the Ebro valley; the upper Douro Valley; the Guadalquivir Valley; at Cape Gata and at the Strait of Gibraltar in summer (Fig. 8(e, f)). Finally, note that the increase of wind speed and wind power at the Strait of Gibraltar is projected practically during the whole year, regardless of the season.

Comparing the obtained wind projections with previous research in the same area is not straightforward since they are strongly dependent on the spatial resolution, the ensemble of RCMs, the scenario and the periods of time considered. A decrease in mean wind speed was projected over land by means of RCMs under the A1B scenario in the Iberian Peninsula and Balearic Islands from 2031 to 2050 [14]. The decrease is less marked in the Atlantic fringe and in the southern tip of the Iberian Peninsula, and stronger in the Mediterranean fringe. The mean wind speed decrease is lesser than 5% analyzing the time

Table 11
Wind increment, ΔW (ms^{-1}), and increment in the number of days with wind speed under the cut-in velocity of 3 ms^{-1}, ΔCalms (# days), from 2006 to 2099. * means that there is consensus between RCMs. There is a consensus when at least two thirds of the models agree in the sign of the increment and at least half of those models have a significance higher than 90%.

# Buoy	ΔW	ΔCalms	# Wind Farm	ΔW	ΔCalms
S1 Bilbao	−0.38*	7	L1 Silvaredonda	0.13	0
S2 Cape Peñas	−0.33*	4	L2 Codesas I	0.05	0
S3 Estaca de Bares	−0.25	1	L3 Codeas II	0.07	−1
S4 Sisargas	0	2	L4 Val de Lín	−0.39*	7*
S5 Cape Silleiro	−0.06	5	L5 Val de la casa	−0.40*	8
S6 Gulf of Cádiz	−0.34*	6	L6 Val de Pero	−0.08	2
S7 Cape Gata	0.08	−1	L7 Montejo	−0.22	0
S8 Cape Palos	−0.16	3	L8 Canredondo	−0.34*	11*
S9 Valencia	−0.31*	4	L9 Peña I	−0.42*	9*
S10 Tarragona	−0.46*	14*	Loma Gorda		
S11 Begur	−0.30*	4	San Gil		
S12 Dragoneras	−0.49*	14*	L10 La Losilla	−0.16	0
S13 Mahon	−0.38*	7*	L11 Malagón I, II	−0.28	4
			L12 Las Vegas	0.32*	−5

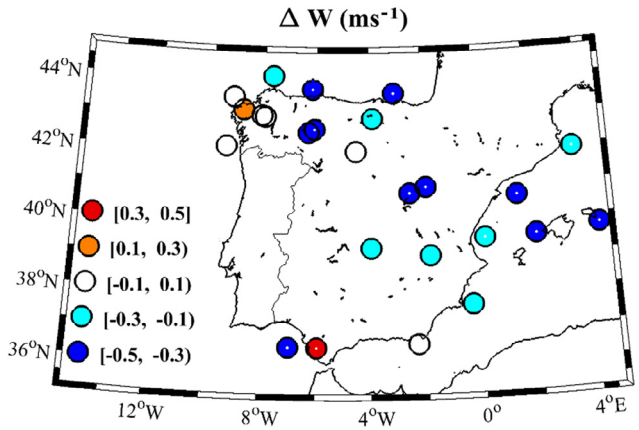

Fig. 5. Wind increment (ΔW, ms^{-1}) from 2006 to 2099. Circles mark the location of wind farms and buoys and white dots inside mark those locations where there is a consensus in the sign and significance of change. There is consensus when at least two thirds of the models agree in the sign of the increment and at least half of those models have a significance higher than 90%.

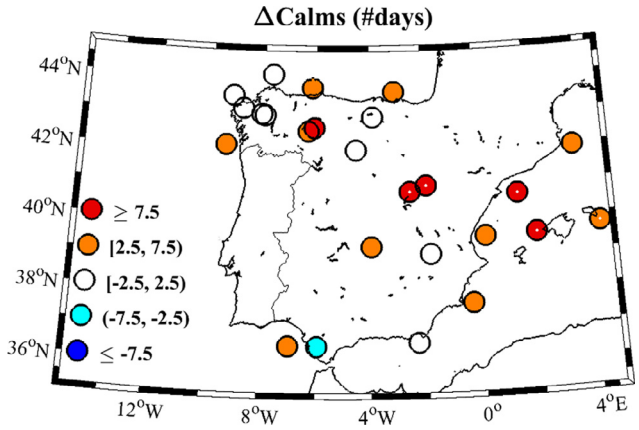

Fig. 6. Increment in the number of days with wind speed under the cut-in velocity of 3 ms^{-1} (ΔCalms, #days) from 2006 to 2099. Circles mark the location of wind farms and buoys and white dots inside mark those locations where there is a consensus in the sign and significance of change. Consensus criterion as in Fig. 5.

evolution of annual averages for the 2005 to 2050 period. Here, a similar overall decrease is observed in most of the areas. Positive spots identified in the present study were not observed in their analysis since they focused on macroscopic clusters. On the other hand, seasonal projections show opposite behaviors in both studies. They found that the majority of seasonal trends are not significant but projected a significant decrease in wind speed in Galicia and at the Strait of Gibraltar during summer for the 2000–2050 period.

The results presented here also agree with those obtained for the Iberian Peninsula by means of the COSMO-CLM RCM driven by the ECHAM5 GCM under the scenario A1B with a spatial resolution of 20 km over the period 2041–2070 [28]. They found a significant decrease in wind potential over most of the peninsula accompanied by an increase in the northwestern Galicia and at Gibraltar Strait throughout the year, and in the Ebro Valley during summer (see their Fig. 3). They relate the enhancement of wind power in northwestern Galicia to the northward displacement of North Atlantic westerly winds during winter and to the intensification of local winds in the Ebro Valley [49].

None of studies mentioned above analyzed changes in offshore winds. Most of the previous studies dealing wind projections offshore the Iberian Peninsula covered larger regions with coarser resolution. In fact, an annual decrease of wind power ranging from −10% to −15% in the Iberian Peninsula and the Bay of Biscay and an increase from 5% to 10% in a small region west of the Strait of Gibraltar were detected [11]. These results are in partial agreement with the findings of the present study. The only apparent discrepancy is observed in Atlantic coast of Galicia, where a clear increasing in wind power was observed in the present study. In fact, the two models considered by [11] show a clear increase in summer that is overbalanced by a stronger decrease in winter. Differences between both studies are probably motivated by several factors: the number of RCMs under scope (nine simulations from CORDEX project in the present study instead of only two RCMs), differences in the spatial resolution (12.5 km in the present study instead of 30–50 km), the different scenarios (RCP8.5 instead of A1B) and, finally, the historical and far future periods considered (1976–2005 and 2070–2099 instead of 1961–2000 and 2061–2100).

Similar changes for the areas that are common to the present study were projected by means of 10 RCMs driven by 6 GCMs under the A1B scenario from the EMSEMBLES project [21]. They analyzed 15 simulations with a spatial resolution of 25 km for two future periods of time (2031–2060 and 2071–2100). Unfortunately, the Atlantic part of the Iberian Peninsula is only partially covered in that study. Even so, positive changes in wind power (on the order of 5–10%) can be observed for the northern part of the WIP and close to the Strait of Gibraltar, in good agreement with the present study (see their Fig. 1).

More recently, [29] analyzed the future offshore wind resource in the Western Iberian by means of an ensemble of RCMs under the RCP4.5 and RCP8.5 scenarios within the framework of the CORDEX project from 2071 to 2100. They found no change in the annual offshore wind power density in the Iberian northwest coast and a reduction of less than 5% for the rest of the western Iberian coast. A discrepancy is observed only for the Atlantic coast of Galicia where an increase is obtained in the present study. Nevertheless, note that the increase detected in the present study is probably in their range of no change (± 2.5%, see their Fig. 8). In fact, their WRF simulations show power density increments between 5% and 7% in the Atlantic coast of Galicia. From the seasonal projection, they obtained a power density reduction of around 7% for winter, 4% for spring and 12% for autumn and an increase of 5% for summer in the Atlantic sea of the Iberian Peninsula. In the latter season, the wind power density increase obtained in the northwest coast is 20%. In the present study, a higher power density reduction (~20%) were projected in winter, a similar wind power reduction (5%) in spring, an increment on the order of 2.5% in a small area in the northwest coast and a reduction (2.5%) for the rest in autumn and finally a similar increment was projected (20%) for summer. Once again, differences between studies can be motivated

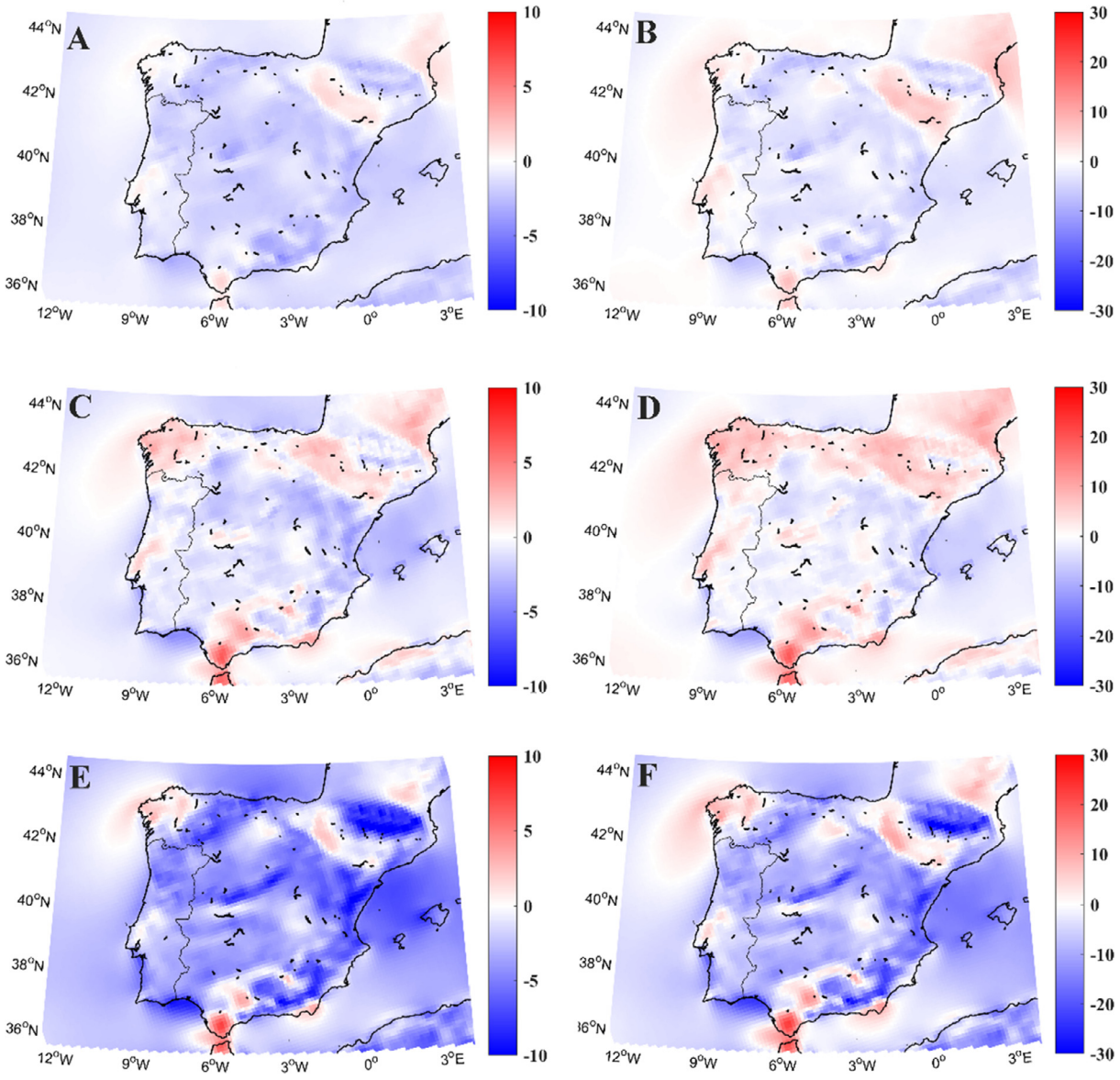

Fig. 7. Map of percentage of change in mean wind speed (in ms^{-1}, left column) and wind power (in Wm^{-2}, right column) projected by means of RCMs from CORDEX under the RCP8.5 scenario for three future periods: (A, B) near future (2019–2045), (C, D) midterm (2046–2072), (E, F) far future (2073–2099). Changes are relative to the historical period (1976–2005).

by different reasons such as: the extrapolation to the hub height of offshore turbines (120 m instead 90 m), the RCMs ensemble, the historical and far future periods considered to calculate increments in wind speed and wind power (1976–2005 and 2073–2099 instead of 1971–2000 and 2071–2100).

4. Conclusions

The skill of CORDEX regional models to reproduce the wind speed over the Iberian Peninsula was analyzed in terms of the percentage of error of the mean wind (EP) and the overlap percentage (OP) at 28 locations placed both inland (15 wind farms) and offshore (13 buoys) during 2012.

Overall, the RMSE of EP was 10% at ocean locations and 19% at inland locations. The bias is slightly positive in both cases (2% and 5%, respectively), which proves the accuracy of models to reproduce the mean wind speed.

In addition, the OP between measured and projected distributions was also analyzed, showing a mean OP of 82 ± 5% for inland locations and 83 ± 3% for offshore locations, showing that RCMs can reproduce with a considerable skill the measured wind distributions at specific locations. The skill is even higher when longer period of time are considered, as proved for buoys over the period 2006–2016. In this way, it can be considered that the CORDEX RCMs are able to realistically represent the wind flow over the areas here considered.

CORDEX RCMs also showed a higher skill than CMIP5 GCMs, both in terms of EP and OP. This is especially patent at near shore buoys, where the coarseness of the GCMs does not allow identifying whether the points are located offshore or inland and where the meteorological dynamics of the land-ocean transition zones is poorly represented.

Once the skill of CORDEX was shown, wind speed was projected for the 21st century showing an overall decrease on the order of 5% at the locations where *in situ* measurements were available, both inland and offshore (Fig. 5). This decrease is less intense in the Atlantic fringe of the Iberian Peninsula where buoys and wind farms show no changes or a light increase; and stronger in the Mediterranean area, in particular around the Balearic Islands, where there is a high consensus on negative trends at all buoys. Consensus in the sign of the trend was observed in

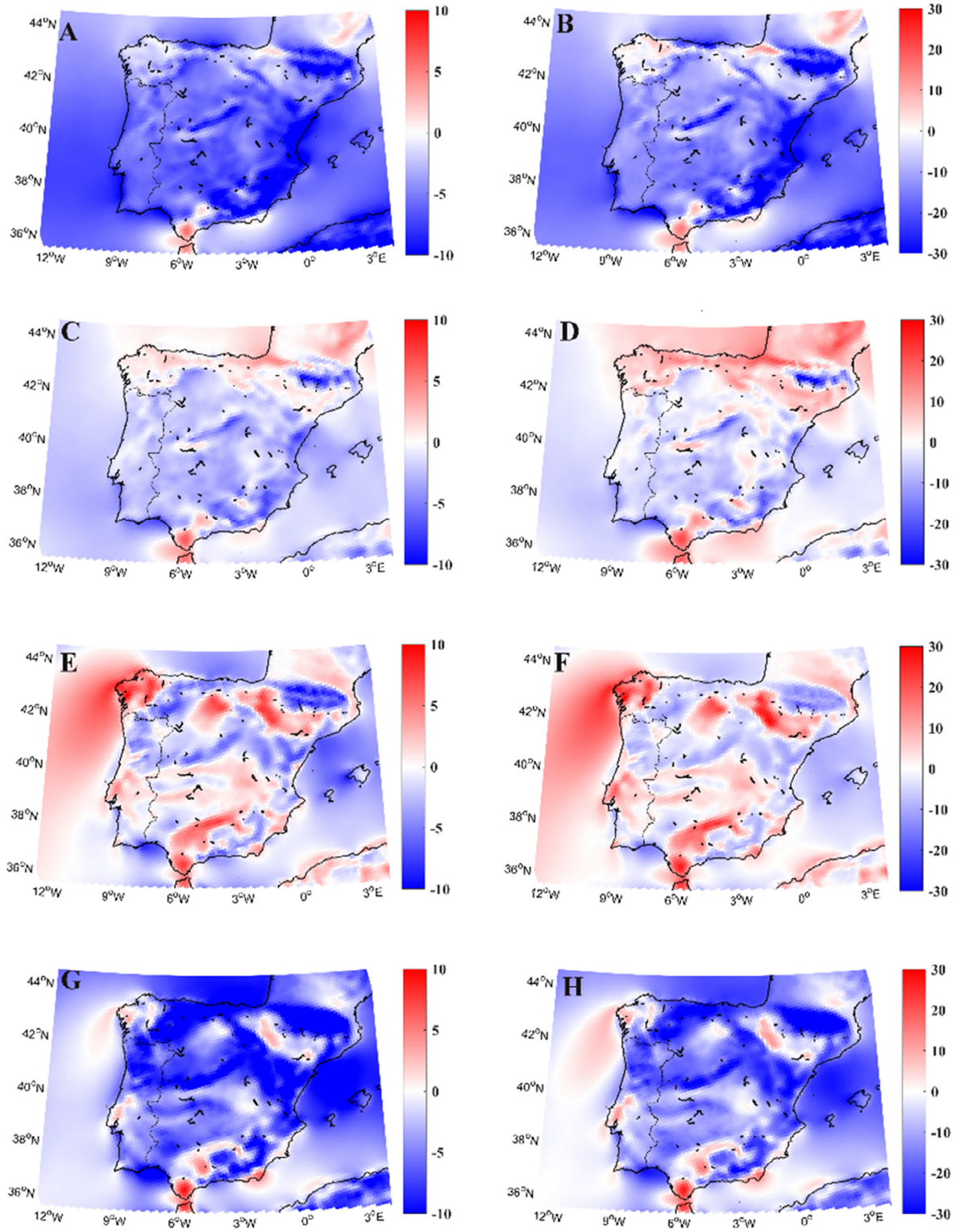

Fig. 8. Map of percentage of change in mean wind speed (left column) and wind power (right column) projected by means of RCMs from CORDEX under the RCP8.5 scenario during: (A and B) winter (DJF); (C and D) spring (MAM); (E and F) summer (JJA) and (G and H) autumn (OND) for the far future (2073–2099). Changes are relative to the historical period (1976–2005).

50% of the buoys but only in 25% of the farms, which is due to the different topography used by every model. Only the wind farm located at the Strait of Gibraltar (station L12) showed a wind increase on the order of 5%, which is, surprisingly, similar in magnitude but opposite in sign to the wind decrease projected at the buoy located in the Gulf of Cadiz. Thus, opposite behaviors were projected at two stations that are less than 1° apart, showing the importance of selecting the right emplacement for wind farms, which can only be done with regional models of fine spatial resolution. Additionally, an increment in the number of days under the cut- in velocity is projected for most of the wind farms and buoys.

Finally, a complete characterization of climate change impact on

Iberian wind resources was carried out both inland and offshore at annual and seasonal scale. Wind speed and power from an ensemble of nine CORDEX RCMs were projected for three future periods: near future (2019–2045), midterm (2046–2072) and far future (2073–2099), all compared to the historical period (1976–2005). A generalized yearly decrease in mean wind speed and power is observed for the entire Iberian Peninsula and Balearic Islands and offshore, both in the occidental Mediterranean Sea and in the Atlantic Ocean with the exception of some particular regions as: Galicia; the Atlantic coast of Galicia and north of Portugal; the Ebro Valley; the upper Douro Valley; the Guadalquivir Valley; the Strait of Gibraltar and Cape Gata, where both wind speed and wind power will tend to increase. This increment is projected to occur mostly during summer with the exception of the Strait of Gibraltar where occurs all year long. The change in wind speed and power is higher as farthest the future period is.

Acknowledgments

Funding: This research was partially supported by Xunta de Galicia under project GRC-2013-001 “Programa de Consolidación e Estructuración de Unidades de Investigación Competitivas (Grupos de Referencia Competitiva)” co-funded by European Regional Development Fund (FEDER). The Portuguese Science Foundation (FCT) partially supported this research through a Postdoctoral grant (SFRH/BPD/97320/2013) of the first author and through the project Pest (C/MAR/LA0017/2013). We thank Gas Natural Fenosa Renovables SLU (https://en.wikipedia.org/wiki/Gas_Natural) for providing part of the data used in this study. Juan A. Añel is supported by a Ramón y Cajal grant by the Government of Spain (RYC-2013-14560).

References

[1] Intergovernmental Panel on Climate Change (IPCC). Fifth assessment report; 2014. http://www.ipcc.ch/report/ar5/.
[2] Global wind report. Annual market update. Global wind energy council (GWEC); 2017. http://www.gwec.net/publications/global-wind-report-2/.
[3] Wind in power. Annual combined onshore and offshore wind energy statistics; 2017. https://windeurope.org/wp-content/uploads/files/about-wind/statistics/WindEurope-Annual-Statistics-2017.pdf.
[4] Wind energy in Europe: Scenarios for 2030 report; 2017. https://windeurope.org/wp-content/uploads/files/about-wind/reports/Wind-energy-in-Europe-Scenarios-for-20130.pdf.
[5] Offshore Wind in Europe. Key trends and statistics; 2017. https://windeurope.org/wp-content/uploads/files/about-wind/statistics/WindEurope-Annual-Offshore-Statistics-2017.pdf.
[6] Añel JA. On the importance of weather and climate change for our present and future energy needs. In: Dubus T, Haupt E, editors. Contemporary physics 2015. p. 206–8. http://dx.doi.org/10.1080/00107514.2015.1006251.
[7] Taylor K. CMIP5 standard- output. http://cmip-pcmdi.llnl.gov/cmip5/docs/standard_output.pdf.
[8] Carvalho D, Rocha A, Gómez-Gesteira M, et al. Potential impacts of climate change on European wind energy resource under the CMIP5 future climate projections. Renew Energy 2017;101:29–40.
[9] Fowler HJ, Blenkinsop S, Tebaldi C. Linking climate change modelling to impacts studies: recent advances in downscaling techniques for hydrological modelling. Int J Climatol 2007;27(12):1547–78. http://dx.doi.org/10.1002/joc.1556.
[10] Koletsis I, Kotroni V, Lagouvardos K, Soukissian T. Assessment of offshore wind speed and power potential over the Mediterranean and the Black Seas under future climate changes. Sustain Energy Rev 2016;60:234–45.
[11] Hueging H, Rabea H, Born K, et al. Regional changes in wind energy potential over Europe using regional climate model ensemble projections. J Appl Meteorol Climatol 2013;52:903–17.
[12] Pryor S-C, Barthelmie R-J, Clausen N-E, et al. Analyses of possible changes in intense and extreme wind speeds over northern Europe under climate change scenarios. Clim Dyn 2012;38:189–208.
[13] Rockel B, Woth K. Extremes of near-surface wind speed over Europe and their future changes as estimated from an ensemble or RCM simulations. Clim Change 2007;81:267–80.
[14] Gómez G, et al. Characterization of the wind speed variability and future change in the Iberian Peninsula and the Balearic Islands. Wind Energ 2016;19:1223–37. http://dx.doi.org/10.1002/we.1893.
[15] González A, Pérez JC, Díaz JP, Expósito FJ. Future projections of wind resource in a mountainous archipelago, Canary Islands. Renew Energy 2017;104:120–8. http://dx.doi.org/10.1016/j.renene.2016.12.021.
[16] Jones C, Giorgi F, Asrar G. The coordinate regional downscaling experiment: CORDEX an international downscaling link to CMIP5. CLIVAR Exch Newsl 2011;16:34–40.
[17] Pryor SC, Barthelmie RJ. Use of RCM simulations to assess the impact change on wind energy availability. Riso-R1477 2004. (EN) Rep. 111; 2004.
[18] Pryor S, Barthelmie R, Kjellstrom E. Potential climate change impact on wind energy resources in northern Europe analyses using a regional climate model. Clim Dyn 2005;25:815–35.
[19] Kjellstrom E, Nikulin G, Hansson U, et al. 21stcentury changes in the European climate: uncertainties derived from an ensemble of regional climate model simulations. Tellus 2011;63A:24–40.
[20] Outten SD, Esau I. Extreme winds over Europe in the ENSEMBLES regional climate models. Atmos Chem Phys 2013;13:5163–72.
[21] Tobin I, Vautard R, Balog I, et al. Assessing climate change impacts on European wind energy from ENSEMBLES high-resolution climate projections. Clim Chang 2015;128(1–2):99–112.
[22] Reyers M. J.G. Pinto & J. Moemken. Statistical-dynamical downscaling for wind energy potentials: evaluation and applications to decadal hindcasts and climate change projections. Int J Climatol 2015;35:229–44. http://dx.doi.org/10.1002/joc.3975.
[23] Davy R, Gnatiuk N, Pettersson L, et al. Climate change impacts on wind energy potential in the European domain with focus on the Black Sea. Renew Sustain Energy Rev 2017. http://dx.doi.org/10.1016/j.rser.2017.05.253.
[24] Bloom A, Kotroni V, Lagouvardos K. Climate change impact of wind energy availability in the Eastern Mediterranean using the regional climate model PRECIS. Nat. Hazards Earth Syst. Sci. 2008;8:1249–57.
[25] Nolan P, Lynch P, McGrath R, et al. Simulating climate change and its effects on the wind energy resource of Ireland. Wind Energy 2012;15:593–608.
[26] Cradden LC, Harrison GP, Chick JP. Will climate change impact on wind power development in the UK? Clim Change 2012;115:837–52.
[27] Sterl A, Bakker A, van den Brink H, et al. Large-scale winds in the southern North Sea region: the wind part of the KNMI’14 climate change scenarios. Environ Res Lett 2015;10(3):035004.
[28] Santos J-A, Rochinha C, Liberato M-L-R, Reyers M, Pinto JC. Projected changes in wind energy potentials over Iberia. Renew Energy 2015;75:68–80.
[29] Soares PMM, Daniela CA, Cardoso R, et al. Western Iberian offshore wind resources: more or less in a global warming climate? Appl. Energy 2017;203:72–90.
[30] Brands S, Herrera S, Fernández J, Gutiérrez JM. How well do CMIP5 earth system models simulate present climate conditions in Europe and Africa? Clim. Dyn. 2013;41:803–17.
[31] Staffell I, Pfenninger S. Using bias- corrected reanalysis to simulate current and future wind power output. Energy 2016;114:1224–39.
[32] Andresen GB, Søndergaard AA, Greiner M. Validation of Danish wind time series from a new global renewable energy atlas for energy system analysis. Energy 2015;93:1074e88.
[33] Olauson J, Bergkvist M. Modelling the Swedish wind power production using MERRA reanalysis data. Renew Energy 2015;76:717e25.
[34] Rose S, Apt J. What can reanalysis data tell us about wind power? Renew Energy 2015;83:963e9.
[35] Carvalho D, Rocha A, Gómez-Gesteira M, et al. A sensitivity study of the WRF model in wind simulation for an area in high wind energy. Environ Modell Softw 2012;33:23–34.
[36] Carvalho D, Rocha A, Gómez-Gesteira M, et al. WRF wind simulation and wind energy production estimates forced by different reanalyses: comparison with observed data for Portugal. Appl Energy 2014;117:116–26.
[37] Carvalho D, Rocha A, Gómez-Gesteira M, et al. Offshore wind energy resource simulation forced by different reanalyses: comparison with observed data in the Iberian Peninsula. Appl Energy 2014;134:57–64.
[38] Carvalho D, Rocha A, Gómez-Gesteira M, et al. Sensitivity of the WRF model wind simulation and wind energy production estimates to planetary boundary layer parametrizations for onshore and offshore areas in the Iberian Peninsula. Appl Energy 2014;135:234–46.
[39] Monin AS, Obukhov AM. Osnovnye zakonomernosti turbulentnogo peremeshivanija v prizemnom sloe atmosfery (Basic laws of turbulent mixing in the atmosphere near the ground). Trudy geofiz inst, AN SSSR 1954;24(151):163–87.
[40] Liu WT, Tang W. Equivalent neutral wind. Pasadena (California): JPL Publication, Jet Propulsion Laboratory, California Institute of Technology; 1996.
[41] Hoogwijk M, De Vries B, Turkenburg W. Assessment of the global and regional geographical, technical and economic potential of onshore wind energy. Energy Econ 2004;26:889–919.
[42] de Lucena A-P Pereira, Szklo A Salem, Schaeffer R, Dutra R Marques. The vulnerability of wind power to climate change in Brazil. Renew Energy 2010;35:904–12.
[43] Engineering Sciences Data Unit. Characteristics of wind speed in the lower layers of the atmosphere near ground: strong winds (neutral atmosphere). London (Regent Street, UK): ESDU; 1972.
[44] Hansen F-V. Surface roughness lengths. Army Research Laboratory; 1994.
[45] Perkins SE, Pitman AJ, Holbrook NJ, McAneney J. Evaluation of the AR4 climate models’ simulated daily maximum temperature, minimum temperature, and precipitation over australia using probability density functions. J Clim 2007;20:4356–76. http://dx.doi.org/10.1175/JCLI4253.1.
[46] Quenouille MH. Associated measurements. London: Butterworth Scientific Publications; 1952. p. 242.
[47] Lima FP, Wethey DS. Three decades of high- resolution coastal sea surface temperatures reveal more than warming. Nat Commun 2012;3:704. http://dx.doi.org/10.1038/ncomms1713.
[48] Sousa MC, deCastro M, Álvarez I, Gómez-Gesteira M, Dias JM. Why coastal upwelling is expected to increase along the western Iberian Peninsula over the next century? Sci Total Environ 2017;592:243–51. http://dx.doi.org/10.1016/j.scitotenv.2017.03.046.
[49] Ramos JG, Cratchley CR, Kay JA, Casterad MA, Martínez-Cob A, Domínguez R. Evaluation of satellite evapotranspiration estimates using groundmeteorological data available for the Flumen District into the Ebro Valley of N.E. Spain. Agric Water Manage 2009;96:638e52.